Geol Rundsch (1994) 83: 564–577

R. J. Stern · A. Kröner · R. Bender · T. Reischmann
A. S. Dawoud

Precambrian basement around Wadi Halfa, Sudan: a new perspective on the evolution of the East Saharan Craton

Received: 27 September 1993 / Accepted: 31 May 1994

Abstract This paper provides new geochemical and isotopic data on the evolution of the western foreland to the Nubian shield of north-east Africa. There is abundant evidence for early to middle Proterozoic crust west of the River Nile, but this was severely affected by the Pan-African (≈ 500–900 Ma) orogenic cycle. The results are reported of Rb–Sr whole rock and zircon evaporation geochronological studies and whole rock Sm–Nd and feldspar Pb isotopic analyses for four rock units around Wadi Halfa in northernmost Sudan. These results indicate the presence of heterogeneous pre-Pan-African crustal components, preserved in mylonitic gneisses and in conglomerates that unconformably overlie the gneisses. Several episodes of crust formation, inferred from zircon ages, are preserved in the gneisses: 2.6, 2.4, 2.0, 1.7, 1.2 and 0.72 Ga. Nd model ages for the same units are invariably older than the zircon ages, yet still record a predominantly late Archaean and Palaeoproterozoic history, with depleted mantle model ages between 1.3 and 2.8 Ga. The earliest recorded Pan-African magmatic event is about 720 Ma and dates the beginning of collisional deformation. A younger Pan-African volcanic sequence (≈ 650 Ma) has isotopic compositions of Sr and Nd compatible with derivation from late Proterozoic asthenospheric mantle. A ≈ 530 Ma anorogenic 'A-type' granite also has isotopic compositions suggesting derivation from a primitive source. The inferred tectonic evolution began with rifting to form an oceanic re-entrant. This was followed by subduction leading to collision at about 700 Ma, accompanied by post-orogenic rifting at about 650 Ma.

Key words Precambrian · Geochronology · Geochemistry · Crustal evolution · Africa

R. J. Stern ✉
Center for Lithospheric Studies, University of Texas at Dallas, PO Box 830688, Richardson TX 75083-0688, USA
Fax: 001-214-690-2829

A. Kröner · R. Bender · T. Reischmann
Institut für Geowissenschaften, Johannes-Gutenberg Universität, Postfach 3980, D-55099 Mainz, Germany

A. S. Dawoud
Department of Geology, University of Khartoum, PO Box 321, Khartoum, Sudan

Introduction

Much of the African crust is made up of Archean and Paleoproterozoic cratons surrounded by younger mobile belts, such as the Kalahari craton, the Congo craton and the West African craton. These blocks were unaffected by the Neoproterozoic Pan-African orogenic cycle (900–550 Ma). In contrast, the vast crustal tract that stretches east–west from the Hoggar and Air Mountains in the Sahara to the Arabian–Nubian Shield (ANS) and north–south from the Congo Craton to the Mediterranean is geologically complex and little known (Fig. 1). Our poor understanding of the evolution of this tract is singularly unfortunate because it encompasses a significant proportion of northern Africa.

There is not even agreement on what this crustal tract should be called. Rocci (1965) named it the 'Nile craton', whereas Bertrand and Caby (1978) and Schandelmeier et al. (1987) called it the 'East Saharan craton'; Kröner (1977) interpreted continuity with the Congo craton and termed it the 'Sahara–Congo craton'. These names are an implicit recognition that older continental crust existed west of the River Nile. However, the term 'craton' is inappropriate because this tract was severely affected by Pan-African intrusions and eruptions, metamorphism and deformation. In the sense that a craton does not experience the deformation and igneous activity during orogenies taking place around its margins, the crust west of the Nile did not behave as a craton during the Pan-African orogenic cycle. Black and Liégeois (1993) argued that this crust was a craton before the Pan-African episode, but was almost totally remobilized during it, and named it the 'Central Saharan Ghost Craton'. However,

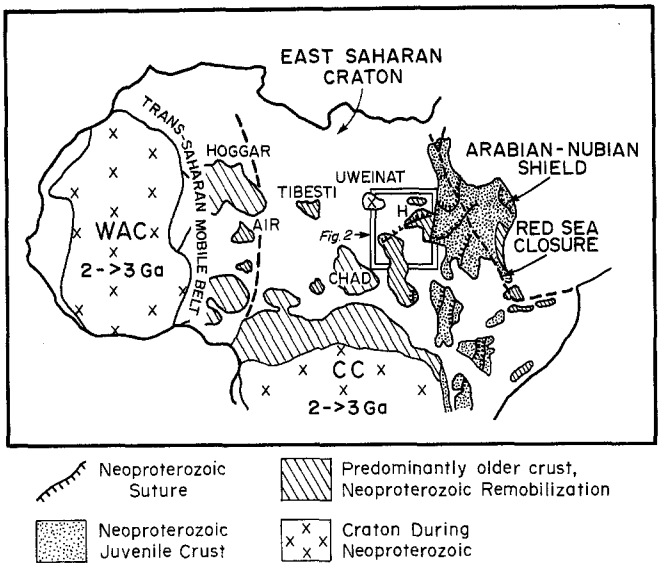

Fig. 1. Generalized map of major Precambrian rock units in northern Africa, showing the threefold subdivision of basement. Continental crust that was formed during the Neoproterozoic is largely restricted to the Arabian–Nubian Shield and its extensions to the south. Older continental crust which behaved as stable foreland during the Neoproterozoic is preserved as the West African craton (WAC) and Congo craton (CC). The diagonally ruled pattern shows the occurrence of crust which often contains isotopic evidence of a pre-Neoproterozoic heritage, but which was intensely affected by the Neoproterozoic Pan-African orogeny, and is referred to in this paper as the East Saharan craton (ESC). From this region, only parts of the Hoggar and a few exposures around Uweinat show no evidence of Neoproterozoic orogenesis. The location of Fig. 2 is shown in the framed box.

this name implies that the region was a craton before the Neoproterozoic, a hypothesis that remains untested. We recognize the weakness in logic for using the term'craton' for the region, but for the purposes of consistency with earlier usage, we will refer in this paper to the region shown by diagonally ruled lines in Fig. 1 as the East Saharan craton (ESC).

To date, only outcrops around Uweinat (Figs 1 and 2) have yielded unequivocal Archean and lower Proterozoic radiometric dates (Rb/Sr whole rock: Klerkx and Deutsch, 1977; U–Pb zircon: Sultan et al., 1994), but the argument that the ESC has a pre Pan-African ancestry is substantiated by several lines of evidence. Sultan et al. (1994) found that an anorthosite at Gebel El Asr (about 150 km north of Wadi Halfa; Fig. 2) has Paleoproterozoic (1.92–2.14 Ga) upper intercept ages and ca. 690 Ma lower intercept age. Dixon (1981) dated two cobbles from the Neoproterozoic Atud formation of south-east Egypt which yielded U–Pb zircon upper intercept ages of ca. 1120 and 1860 Ma. Dixon (1979) reported another cobble with a U–Pb zircon upper intercept age of ca. 2.3 Ga. These clasts were interpreted to have been derived from west of the present Nile. Single grain dating of zircons isolated from Neoproterozoic metasediments in the Eastern Desert of Egypt yielded ages between 760 Ma and 2.65 Ga; these were also interpreted to have been eroded from older crust west of the Nile (Wust et al., 1987; Wust 1989). Various rocks in the south-western part of the south-eastern Desert of Egypt have yielded old ages, including 3.0 Ga xenocrystic zircons in 770 Ma old dykes (Kröner et al., 1992) and 1.46 Ga and 2.40–2.45 Ga detrital zircons in sediments (Wust, 1989) along the western part of the Allaqi suture and pelitic metasediments farther north yielding T_{DM} = 1.8 Ga (Harris et al., 1984). Farther south at Sabaloka (Fig. 2), Kröner et al. (1987a) studied metasedimentary granulites that formed about 720 Ma ago and contain detrital zircons as old as 2.6 Ga, and inferred that these granulites formed near the boundary between juvenile, ensimatic terranes of the ANS and pre-Pan-African crust to the west. Sultan et al. (1990) documented 1.6 Ga xenocrystic zircons in the Nakhil granite of north-eastern Egypt but could not resolve whether this indicated the role of old crust or sediments shed from the ESC.

Nd isotopic studies have proved useful in distinguishing between juvenile ANS crust and reworked crust of the ESC. Harris et al. (1984), Schandelmeier et al. (1987) and Harms et al. (1990) reported Paleoproterozoic and late Archean Nd model ages (T_{DM}) for a wide variety of lithologies along and west of the Nile (Fig. 2); these samples yield Neoproterozoic Rb–Sr whole rock ages, albeit generally with high initial $^{87}Sr/^{86}Sr$ (R_i). It is on the basis of these studies and the feldspar Pb isotopic work of Sultan et al. (1992a) that the ESC-ANS boundary can be approximated along the Nile (Figs 1 and 2).

In the Red Sea Hills (RSH) of the Sudan, the island arc domains are separated from each other by belts of strong deformation containing variously preserved and frequently tectonically dismembered ophiolite complexes. Kröner et al. (1987b) have suggested that these belts represent sutures along which the various arcs were welded together, in analogy with the accretion model developed for similar rocks in the Arabian shield (Camp, 1984; Pallister et al., 1988). Kröner et al. (1987b) also subdivided the RSH into a number of arc terranes separated from each other by the above sutures (Fig. 2) and the north-westernmost of these juvenile terranes was named the Gabgaba terrane after Wadi Gabgaba, a major tributary of Wadi Allaqi (Fig. 2). The western part of this terrane consists of poorly exposed rocks in a mostly flat region between Wadi Amur and the River Nile. Isolated outcrops of quartzite and carbonate sediments, unusual or lacking in the arc associations farther east, suggests a continental margin environment and, on account of the distribution of these rocks, Kröner et al. (1987b) suggested the edge of the African craton to occur in a broad region extending from east of Aswan in Egypt to east of Abu Hamed where the River Nile makes a large loop (Fig. 2). The region within this loop was tentatively considered to be occupied by pre-Pan African basement, mainly on account of descriptions and age data reported by Ries et al. (1985). This account has been mostly confirmed, with a thick sequence of carbonate rocks (Bailateb group; Stern et al., 1993) lying west of the Keraf suture (Fig. 2) and the Atmur-Delgo ophiolite belt (ADOB; Fig. 2) separating the continental Wadi Halfa terrane in the north from

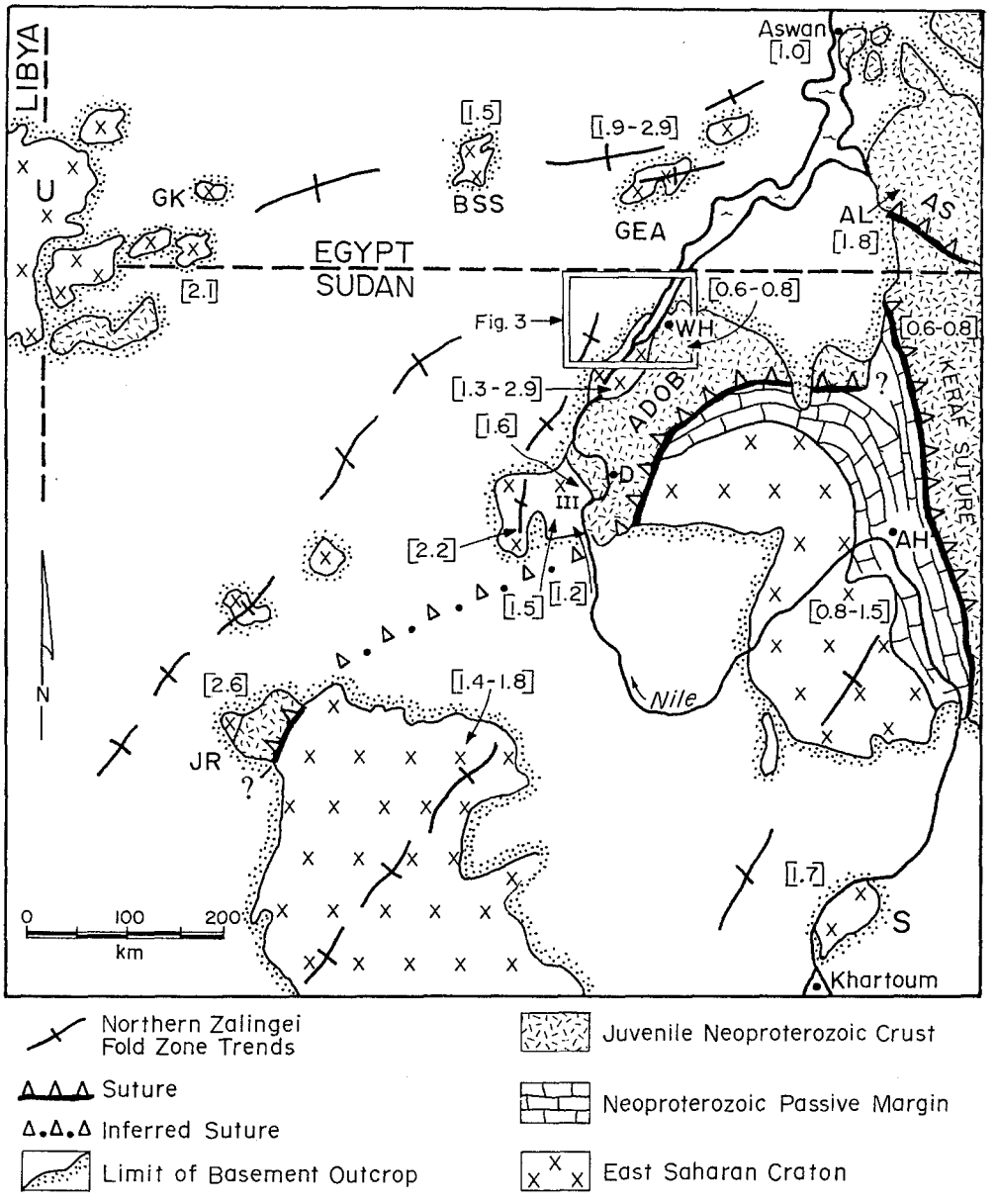

Fig. 2. Generalized geological map of north-central Sudan, modified after Schandelmeier et al. (1987), Griffiths et al. (1987), Denkler et al. (1994) and Schandelmeier et al. (1994). Towns of interest are shown with a dot: WH = Wadi Halfa, D = Delgo, AH = Abu Hamed. Other abbreviated localities: U = Uweinat; GK = Gebel Kamil; BSS = Bir Safsaf; GEA = Gebel El Asr; JR = Jebel Rahib; S = Sabaloka. AS = Allaqi suture; ADOB = Atmur-Delgo ophiolite belt, shown with its inferred extension to the Jebel Rahib area in the southwest. III = Third cataract region. AL = location of metasedimentary sample AL-16 studied by Wust (1989) and approximate location of pelitic metasediments yielding T_{DM} Nd model age of 1.8 Ga (Harris et al., 1984). T_{DM} Nd model ages are in brackets (Harris et al., 1984; Kröner et al., 1987a; Harms et al., 1990; Sultan et al., 1990; Stern and Kröner, 1993; this study). Box delimits the outlines of Fig. 3

the Bayuda terrane in the south (Schandelmeier et al., 1994).

To better define the boundary between the Pan-African and older rocks we undertook an exploratory trip to northern Sudan in 1985 as part of a joint project with the Geological Research Authority of the Sudan and the University of Khartoum. This reconnaissance survey led us from Wadi Amur in the central RSH to the River Nile, then north to Abu Hamed and from there, following the railroad track, to Wadi Halfa. We explored the geology of the region south of Wadi Halfa and the region around the old gold mine of Duweishat on the River Nile, using geological base maps prepared on the basis of a UNDP-sponsored geological study of the Egypt–Sudan Area of Integration (Griffiths et al., 1987). During this survey we collected a number of rock samples for geochemical and geochronological work, the results of which are reported in this paper. The location of these samples is given in Fig. 3. We report here the chemical composition and Rb–Sr whole rock and single grain zircon evaporation ages and the initial isotopic composition of Sr, Nd and Pb of these rocks, which we interpret to provide new insights into the evolution of the easternmost ESC and its relationship with the ANS.

Geological overview and regional relationships

Very little earlier work exists regarding the basement geology around Wadi Halfa. Based on the interpretation of Landsat images in conjunction with the UNDP-sponsored geological study of the Egypt–Sudan Area of Integration, Griffiths et al. (1987) showed the region in Fig. 3 to consist of a paragneiss–orthogneiss terrane along the Nile and to the west, succeeded eastwards by

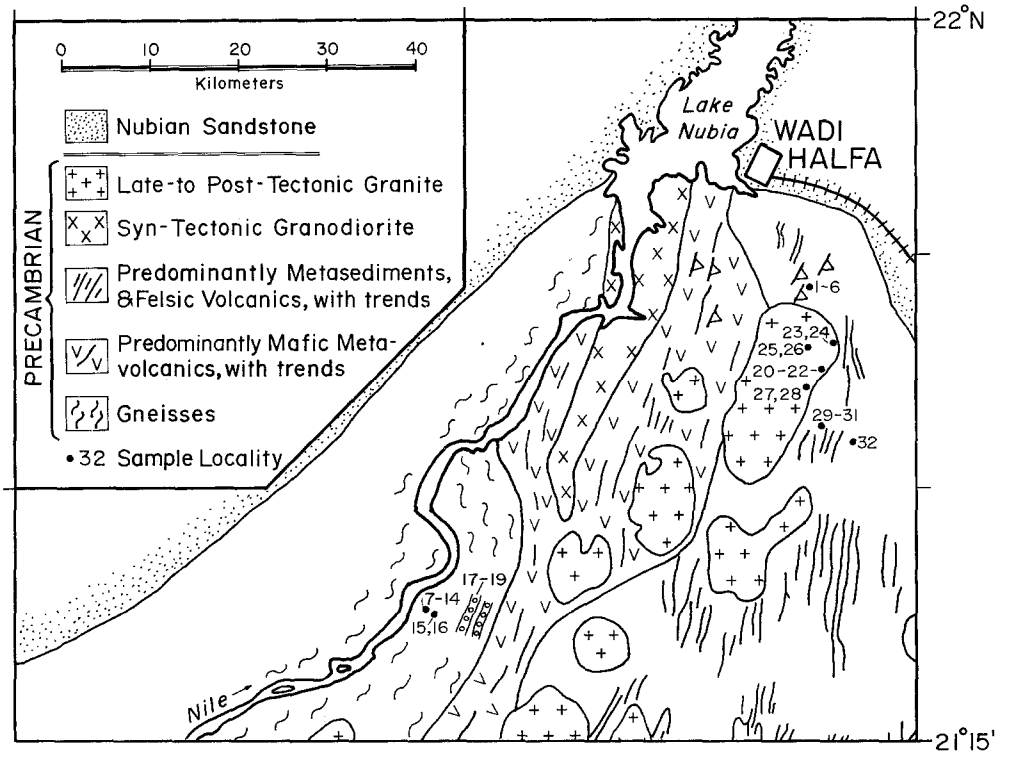

Fig. 3. Sketch map showing the general geological relationships in the basement exposures south of Wadi Halfa and the location of samples studied here

a narrow strip of low grade, dominantly metavolcanic rocks, which is itself succeeded to the east and south by low grade, mostly metasedimentary rocks. Our field investigations indicate that the basement is composed of five principal lithologies: (1) a strongly foliated gneissic terrane in the south and west, which we examined and sampled on a traverse to the Nile near the Duweishat gold mine (Duweishat gneisses). This is unconformably overlain by a less deformed supracrustal succesion, including (2) a succession of principally mafic metavolcanics and (3) farther east, a succession of metasediments and predominantly felsic metavolcanics (Fig. 3), which we sampled at two localities. These three units are intruded by (4) syntectonic granodiorite and (5) post-tectonic alkali granites, one of the latter of which we sampled.

The structure is complex, with mesoscopic tight folding along predominantly north–south axes affecting both gneissic and supracrustal units. The gneiss is heterogeneous, with interlayered metasedimentary (quartzite, carbonate, pelite) rocks and gneisses with igneous precursors. There is good evidence (polymict conglomerate, truncated bedding, differences in styles and intensities of deformation) that an angular unconformity existed between the gneiss and the supracrustal succession, although this is now obliterated by deformation. Earlier structures are also recorded in the gneiss. These linear structures are subparallel to trends reported for the NE–SW to north–south trending Northern Zalingei fold zone in this region (Fig. 2; Vail, 1976; Schandelmeier et al., 1987). The only detailed structural study in this region is that of Vail et al. (1973), in the vicinity of the Third Cataract (Fig. 2). There, metamorphosed sediments, now biotite gneisses, have north–east dipping foliations that were folded around NW–SE trending axes (F_2), F_1 only being visible in hand specimen. F_3 is a more open NE–SW fold set which also affected greenschist facies metavolcanics to the east. These results indicate that the inferred NE–SW trend of the North Zalingei fold zone (Fig. 2), although a good first approximation of structural trends, may be an oversimplification of this polydeformed region.

The lithostratigraphic succession of the study area is similar to that deciphered north of Delgo (Fig. 2), where Denkler et al. (1994) reported an east-facing sequence, with amphibolite facies ortho- and paragneisses, overlain across a sheared unconformity by metasediments (including metaconglomerates) of the Sulb unit. To the east, the Sulb unit is unconformably overlain by greenschist facies metasediments of the Agula unit and then by the metavolcanics of the Abu Sari unit. Using the regional map of Griffiths et al. (1987; Fig. 6), the lithostratigraphy to the south can be correlated with that around Wadi Halfa. Specifically, the Duweishat gneisses correlate with the 'high grade migmatitic basement' west of Delgo and the paragneisses around the Third Cataract, the conglomerates to the east probably correlate with the Sulb unit and the mafic and felsic volcanics farther east correlate with the Abu Sari unit and with the greenschist facies metavolcanics east of the Third Cataract (Vail et al., 1973).

No previous geochronological or isotopic work has been reported for the rocks of the immediate area, but some results are reported for rocks in the vicinity of Wadi Halfa. Near Delgo, about 150 km south of Wadi Halfa (Fig. 2), Harms et al. (1991) reported a Pb–Pb zircon evaporation age for an I-type granodiorite of 731 ± 12 Ma. This body also yielded a T_{DM} Nd model age

Table 1. Geochemistry of Wadi Halfa basement samples: Duweishat 'gneisses'

Oxide (%)	WH-7	WH-8	WH-9	WH-10	WH-11	WH-12	WH-14	WH-15
SiO_2	70.37	58.06	55.61	55.25	59.60	75.56	62.69	59.73
TiO_2	0.24	0.99	1.08	0.83	0.37	0.13	0.66	0.77
Al_2O_3	15.95	17.07	18.93	17.65	18.98	13.92	17.57	17.54
Fe_2O_3	0.94	3.41	1.58	2.40	2.15	0.79	1.84	1.36
FeO	1.22	2.96	5.20	4.21	2.86	0.44	3.30	3.86
MnO	0.04	0.07	0.09	0.08	0.06	0.03	0.11	0.10
MgO	0.92	2.14	3.77	4.91	2.36	0.37	1.56	3.13
CaO	3.12	4.80	7.65	6.78	5.06	1.74	4.09	6.07
Na_2O	3.64	3.15	2.73	2.65	3.95	4.10	3.55	3.60
K_2O	2.63	4.12	1.66	2.62	2.63	2.00	2.95	1.64
P_2O_5	0.07	0.61	0.24	0.33	0.27	0.03	0.36	0.14
H_2O^+	0.84	0.97	1.41	1.41	1.14	0.07	1.09	1.38
H_2O^-	0.11	0.10	0.11	0.08	0.10	0.07	0.13	0.14
CO_2	0.55	1.25	0.64	1.20	0.75	0.59	0.64	1.25
Total	100.64	99.70	100.70	100.40	100.28	100.67	100.54	100.71
Ba (ppm)	1225	2865	434	409	940	1052	560	478
Rb	66	92	40	53	64	47	61	42
Sr	309	840	547	558	665	234	273	349
Nb	8	17	6	6	5	11	11	8
Zr	86	391	65	143	259	75	285	136
Y	11	34	19	18	21	11	25	20
V	20	65	121	134	55	9	25	105
Co	5	12	25	22	10	< 3	8	17
Cr	8	21	23	77	49	12	7	22
Ni	7	24	21	73	25	6	4	20
Ga	13	20	21	21	22	12	20	18
Pb	27	52	11	9	27	46	12	14
Th	6	38	<4	<4	<4	12	<4	6

of 1.6 Ga. Granites and gneisses from west of Delgo yielded Rb/Sr whole rock errorchron ages of 620–920 Ma, with initial $^{87}Sr/^{86}Sr$ (R_i) = 0.706–0.716; a post-tectonic granite yielded a Rb/Sr whole rock isochron age of 565 ± 8 Ma (R_i = 0.7064 ± 2; Harms et al., 1990). These rocks also have T_{DM} Nd model ages of 1.2–2.2 Ga (Harms et al., 1990). At Gebel El Asr, about 150 km to the north in Egypt, Sultan et al. (1994) report that anorthosites have zircons with upper Concordia intercept ages of 1.92 and 2.14 Ga and lower intercept ages of 689 ± 3 Ma. Neodymium model ages for the Gebel El Asr basement indicate a mixed but ancient protolith (T_{DM} = 1.9, 2.5 and 2.8 Ga; Harms et al., 1990; Sultan et al., 1994). Granite and gneiss in and south of Aswan yielded U–Pb zircon ages of 594 ± 4, 634 ± 4 and 741 ± 3 Ma, respectively; Stern and Hedge, 1985; Sultan et al., 1994) and T_{DM} Nd model ages of 1.0 Ga (Harris et al., 1984). These isotopic indications for the presence of older crust contrast with the situation farther east in the ANS where T_{DM} Nd model ages are virtually identical to Rb/Sr whole rock and U–Pb zircon ages of 600–850 Ma, and R_i are consistently ≦ 0.703 0 (Stern and Kröner, 1993).

Analytical techniques

Major and trace element abundances were determined at Mainz by routine XRF techniques (Tables 1 and 2). Rb and Sr concentrations for geochronological purposes were determined by XRF at Mainz following the method of Pankhurst and O'Nions (1973). Sm and Nd concentrations for all samples and Rb and Sr concentrations for two samples were determined by isotope dilution at the University of Texas at Dallas (UTD). Analytical uncertainty for Rb/Sr is about 1.5% and about 1% for Sm/Nd. Analyses for $^{87}Sr/^{86}Sr$ were for the most part carried out using a Shields-type 12″ radius thermal ionization mass spectrometer at UTD, but two additional samples were analysed using the UTD Finnigan MAT 261 thermal ionization mass spectrometer (Table 3). Regression analysis to evaluate the Rb–Sr isotopic data followed York (1969). Errors on ages and initial ratios are given at the 2σ level. In the case of errorchrons (MSWD > F variate), York-II uncertainties have been multiplied by $(MSWD)^{1/2}$.

Seven samples were dated using the single zircon evaporation technique (Kober, 1986; 1987) using a Finnigan MAT 261 mass spectrometer at the Max Planck Institut für Chemie in Mainz. Analytical procedures are detailed in Kröner et al. (1992) and the data are reported in Table 4. In all but two instances, several grains were analysed from each sample and the mean age calculated from these analyses (printed in bold in Table 4) is taken to most closely reflect the time of formation of the respective zircon population. Samples analysed for $^{143}Nd/^{144}Nd$ were dissolved in Krogh-type pressure bombs (Krogh, 1973) at 190°C and Nd was isolated using standard chromatographic (cation exchange followed by further purification using a technique modified after that of Richard et al., 1976) procedures.

Table 2. Geochemistry of Wadi Halfa basememt samples: volcanic rocks, conglomerate clasts, alkali granite

	Volcanic rocks								Volcanic Rocks		Conglomerate clasts			
Oxide (%)	WH-1	WH-2	WH-3	WH-4	WH-5	WH-6	WH-29	WH-30	WH-31	WH-32	WH-17	WH-18	WH-19	Mean alkali granite*
SiO_2	75.76	51.41	78.08	76.90	79.10	77.89	77.69	78.10	77.59	65.04	76.15	76.17	69.42	76.3 ± 0.47
TiO_2	0.26	1.31	0.19	0.18	0.16	0.27	0.13	0.14	0.13	0.97	0.21	0.22	0.49	0.26 ± 0.04
Al_2O_3	12.87	17.00	11.92	12.71	12.38	12.52	12.46	12.60	12.45	15.70	13.20	13.36	14.78	10.7 ± 0.44
Fe_2O_3	1.56	3.67	0.91	0.85	0.85	1.63	0.88	0.84	0.89	2.25	0.77	0.67	1.32	4.2 ± 0.59
FeO	0.75	5.92	1.35	1.09	0.85	0.53	0.96	0.70	0.98	2.47	0.80	0.81	2.23	0.26 ± 0.14
MnO	0.06	0.16	0.05	0.05	0.03	0.11	0.30	0.04	0.06	0.09	0.03	0.03	0.06	0.11 ± 0.04
MgO	0.17	4.87	0.39	0.55	0.28	0.26	0.08	0.07	0.06	1.69	0.66	0.47	2.08	0.08 ± 0.01
CaO	0.59	8.18	0.59	0.64	0.19	0.29	0.26	0.20	0.46	3.32	2.67	3.11	2.69	0.35 ± 0.14
Na_2O	4.71	2.19	4.52	4.60	4.58	3.98	4.21	3.87	4.62	4.81	2.84	2.99	2.65	3.4 ± 0.47
K_2O	2.99	2.11	1.22	1.45	1.42	1.91	2.96	3.41	2.80	1.79	2.26	1.68	3.60	4.0 ± 0.16
P_2O_5	0.03	0.23	0.02	0.02	0.02	0.03	0.01	0.01	0.01	0.27	0.04	0.03	0.11	0.02 ± 0.01
H_2O^+	0.48	3.13	0.86	0.83	0.76	1.05	0.33	0.41	0.15	0.89	0.36	0.34	0.75	–
H_2O^-	0.07	0.12	0.10	0.16	0.09	0.11	0.13	0.12	0.08	0.13	0.19	0.14	0.16	–
CO_2	0.23	0.06	0.46	0.70	0.05	0.09	0.34	0.09	0.34	0.75	0.38	0.54	0.17	–
Total	100.53	100.36	100.66	100.73	100.76	100.67	100.74	100.60	100.62	100.17	100.56	100.56	100.51	99.68
Ba (ppm)	510	475	260	279	294	667	593	775	622	405	913	622	1044	359 ± 188
Rb	35	32	16	19	19	24	36	38	37	23	42	26	77	54 ± 16
Sr	43	302	46	39	44	38	28	33	21	271	272	279	251	12 ± 4
Nb	12	3	13	13	13	11	9	10	10	6	8	8	10	41 ± 12
Zr	380	95	465	334	305	319	341	348	349	225	140	181	156	892 ± 329
Y	63	26	65	70	66	60	44	33	49	29	16	22	18	94 ± 53
V	7	213	9	10	10	15	5	6	6	83	22	21	59	7 ± 1.4
Co	<3	35	<3	3	<3	3	<3	<3	<3	9	3	<3	9	3 ± 1.6
Cr	12	10	13	12	10	10	15	12	12	13	16	19	58	7 ± 2.8
Ni	4	32	4	4	3	4	5	4	3	7	7	5	23	5 ± 0.8
Ga	18	21	17	20	17	10	18	18	19	18	9	13	15	28 ± 3
Pb	9	6	5	5	10	7	13	11	12	9	20	20	20	10 ± 3
Th	4	<4	<4	<4	4	<4	7	6	4	<4	20	19	10	6 ± 2

* Mean alkali granite WH 20–24, 27, 28 (±1 standard deviation).

Analyses were conducted using the UTD Finnigan MAT 261 instrument in the dynamic mode; these results, along Nd and Sm concentrations, $\varepsilon_{Nd}(t)$, and T_{DM} 'crust formation' model ages (Nelson and DePaolo, 1985) are given in Table 5. Calculations of $\varepsilon_{Nd}(t)$ and T_{DM} were made assuming Bulk Earth $^{147}Sm/^{144}Nd = 0.1967$ and using the determinations of ε_{Nd} reported (Pier et al., 1989) for the La Jolla standard (−15.2) and BCR-1 (−0.16) to calculate a Bulk Earth $^{143}Nd/^{144}Nd$ appropriate for the UTD laboratory, where La Jolla $^{143}Nd/^{144}Nd = 0.511847$ and BCR-1 $^{143}Nd/^{144}Nd = 0.512612$. All values were normalized to $^{146}Nd/^{144}Nd = 0.7219$. The total range of ±0.000020 for the standards is taken as the analytical uncertainty.

Potassium feldspar was separated from three samples and analysed for Pb isotopic composition (Table 6). The feldspars were rinsed overnight in 6 M HCl and for 30 minutes in 5% HF to remove labile Pb. The residues were dissolved in HF and Pb isolated. The analyses were corrected for 0.15%/amu for thermal fractionation. Replicate analyses of NBS 981 yielded the following Pb isotopic composition: $^{206}Pb/^{204}Pb = 16.957 \pm 0.11\%$ (total range); $^{207}Pb/^{204}Pb = 15.512 \pm 0.14\%$; $^{208}Pb/^{204}Pb = 36.790 \pm 0.20\%$. Total processing blanks were < 2 ng Sr, < 2 ng Nd and < 1 ng Pb (for feldspars), which are in all instances negligible.

Results

Duweishat gneisses

In the field these rocks appear pink to black in color, are isoclinally folded and have a strong subhorizontal, almost mylonitic, foliation. The lack of centimeter scale compositional banding led us to infer that these are orthogneisses. Samples WH-7 to WH-14 were collected from along a track just west of the Duweishat gold mine, about 200 m apart. WH-15 was collected from similar rocks but a few kilometers farther east. In thin section, these rocks appear fine grained, with strongly strained quartz and other indications of mylonitization. Bender (1991) reported that the gneisses are dominated by biotite, quartz and potassium feldspar, with subordinate plagioclase, hornblende, epidote and muscovite. Samples WH-9, 10 and 15 have green metamorphic hornblende, indicating a temperature of 275–500°C (greenschist facies; Bender, 1991). Major element analyses show that these rocks are intermediate to felsic in composition (55–76% SiO_2). They are enriched in incompatible elements such as K_2O (1.6–4.1%) and Ba (400–2900 ppm), but these enrichments do not covary with SiO_2. For example, WH-8 (SiO_2 = 58%) has by far the greatest abundance of K,

Table 3. Rb–Sr and $^{87}Sr/^{86}Sr$ data for isochron calculations

Sample	Rb (ppm)	Sr (ppm)	$^{87}Rb/^{86}Sr$	$^{87}Sr/^{86}Sr$*
WH-1	35	44.2	2.29	0.72405 ± 5
WH-2	32	304	0.305	0.70530 ± 5
WH-3	16	46.5	0.996	0.71198 ± 7
WH-4	19	41.3	1.34	0.71502 ± 7
WH-6	24	39.3	1.77	0.71934 ± 16
WH-7	66	315	0.607	0.71513 ± 8
WH-8	92	850	0.313	0.71507 ± 7
WH-9+	40.3	566	0.206	0.70830 ± 4
WH-10	53	584	0.263	0.70908 ± 6
WH-11+	64.3	687	0.271	0.71337 ± 4
WH-12	47	236	0.578	0.71940 ± 10
WH-14	61	369	0.479	0.71571 ± 8
WH-15	42	359	0.339	0.71101 ± 7
WH-20	44	10.8	11.84	0.79508 ± 8
WH-21	55	10.4	15.54	0.82497 ± 9
WH-22	34	19.4	5.08	0.74675 ± 6
WH-23+	55	15.2	10.52	0.76098 ± 10
WH-25	65	70.6	2.67	0.72744 ± 8
WH-27	82	9.32	25.95	0.90462 ± 18
WH-28	63	8.09	22.90	0.87939 ± 13
WH-29	36	28.8	3.63	0.73475 ± 9
WH-30	38	33.5	3.29	0.72985 ± 12
WH-31	37	22.2	4.85	0.7425 ± 2
WH-32	23	272	0.245	0.70510 ± 7

* Adjusted for E&A $SrCO_3$ = 0.70800.
+ All samples except these had Rb/Sr determined by XRF at Mainz and were analysed for $^{87}Sr/^{86}Sr$ using the 12″ radius instrument at UTD; quoted errors are in-run precision. These samples had Rb, Sr contents determined by isotope dilution and were analysed for $^{87}Sr/^{86}Sr$ using the Finnigan MAT instrument at UTD; accuracy on $^{87}Sr/^{86}Sr$ for these is ±0.00004.
‡ This point omitted from isochron calculation because it falls far off the isochron.

Rb, Sr, Ba, Nb, Th and Pb, whereas felsic samples WH-7 and 12 have considerably lower abundances of incompatible elements. The succession thus does not appear to be an igneous sequence related by fractionation. Bender (1991) interpreted these as metamorphosed andesites and more felsic rocks. Two felsic samples plot in the field of volcanic arc granites (VAG) on discriminant diagrams designed for use with granitic rocks (Fig. 4).

The geochronological and isotopic results confirm that the Duweishat gneisses are a heterogeneous assemblage of pre-Neoproterozoic ancestry. Rb–Sr whole rock geochronology yields an errorchron of about 2.5 Ga, but one that nevertheless indicates an old age (Fig. 5). The model age for the 'youngest' data point is about 1.4 Ga (R_i assumed = 0.703) and all of the data points are much more radiogenic than would be expected for Neoproterozoic rocks. Single zircon $^{207}Pb/^{206}Pb$ ages for five samples (WH-7 to WH-12; Table 4) indicate an age range that nearly spans the Proterozoic, from ≈ 720 to ≈ 2400 Ma. All zircons analysed were euhedral, with no recognizable cores or obvious overgrowths, and multiple analyses of up to five grains from a single sample (e.g. WH-8) yielded the same age. These observations suggest that the zircons are igneous in origin.

Table 4. Pb isotopic data from single zircon evaporation

Sample number	Grain	Mass scans*	Evaporation temperature (°C)	Mean $^{207}Pb/^{206}Pb$+ and 2σ error	$^{207}Pb/^{206}Pb$ age and 2σ error
WH-7	1	66	1532	0.08145 ± 28	1232 ± 14
	2	65	1529	0.08145 ± 26	1233 ± 12
	1&2	131		0.08145 ± 28	**1232 ± 13**
WH-8	1	88	1554	0.15734 ± 50	2427 ± 6
	2	108	1538	0.15739 ± 61	2428 ± 7
	3	88	1546	0.15747 ± 47	2429 ± 5
	4	66	1530	0.15746 ± 59	2429 ± 6
	5	86	1535	0.15758 ± 81	2430 ± 9
	1–5	436		0.15745 ± 63	**2428 ± 7**
WH-9	1	99	1555	0.06332 ± 20	719 ± 13
	2	121	1565	0.06333 ± 20	720 ± 13
	3	44	1578	0.06333 ± 23	719 ± 16
	1–3	264		0.06333 ± 21	**719 ± 14**
WH-11	1	100	1557	0.15556 ± 40	2408 ± 9
	2	99	1562	0.15524 ± 41	2404 ± 9
	1&2	199		0.15540 ± 44	**2406 ± 10**
WH-12	1	108	1534	0.10667 ± 35	1743 ± 12
	2	88	1526	0.10670 ± 31	1744 ± 10
	1&2	196		0.10668 ± 33	**1744 ± 11**
WH-17‡	1	50	1553	0.06328 ± 40	718 ± 15
WH-19	1	28	1546	0.15951 ± 39	2451 ± 5

* Number of $^{207}Pb/^{206}Pb$ ratios evaluated for age assessment.
+ Observed mean ratio, corrected for non-radiogenic Pb where necessary. Errors based on uncertainties in counting statistics.
‡ Analytical data from Wust (1989).
Bold numbers indicate mean ages calculated from several zircon analyses from the same sample.

Table 5. Sm–Nd isotopic data

Sample	Nd (ppm)	Sm (ppm)	$^{147}Sm/^{144}Nd$	$^{143}Nd/^{144}Nd$	$\varepsilon_{Nd}(T)$*	T_{DM}
WH-7	14.3	2.34	0.0988	0.51121	−19	2.42
WH-8	117	17.5	0.0903	0.51077	−27	2.81
WH-9	18.7	4.11	0.133	0.51202	−6.1	1.90
WH-10	29.5	5.25	0.108	0.51215	−1.3	1.26
WH-11	33.3	6.25	0.114	0.51119	−21	2.82
WH-12	19.5	3.00	0.0928	0.51113	−20	2.40
WH-14	26.3	5.06	0.116	0.51173	−10	2.03
WH-3+	45.5	10.7	0.143	0.51273	+6.6	0.66
WH-22‡	61.5	13.5	0.132	0.51265	+4.9	0.72

Relative to La Jolla $^{143}Nd/^{144}Nd$ = 0.511847 and BCR-1 $^{143}Nd/^{144}Nd$ = 0.512612.
* ε_{Nd} calculated at 700 Ma.
+ ε_{Nd} calculated at 650 Ma.
‡ ε_{Nd} calculated at 530 Ma.

Table 6. Wadi Halfa Feldspar Pb data

Sample No.	$^{206}Pb/^{204}Pb$	$^{207}Pb/^{204}Pb$	$^{208}Pb/^{204}Pb$	Lithology	Age (Ma)
WH-7	16.894	15.715	38.375	Gneiss	1232*
WH-12	17.046	15.774	38.634	Gneiss	1744*
WH-24	18.646	15.555	38.395	Granite	530+

* Kober zircon evaporation Pb/Pb age.
+ Rb–Sr whole rock isochron age.

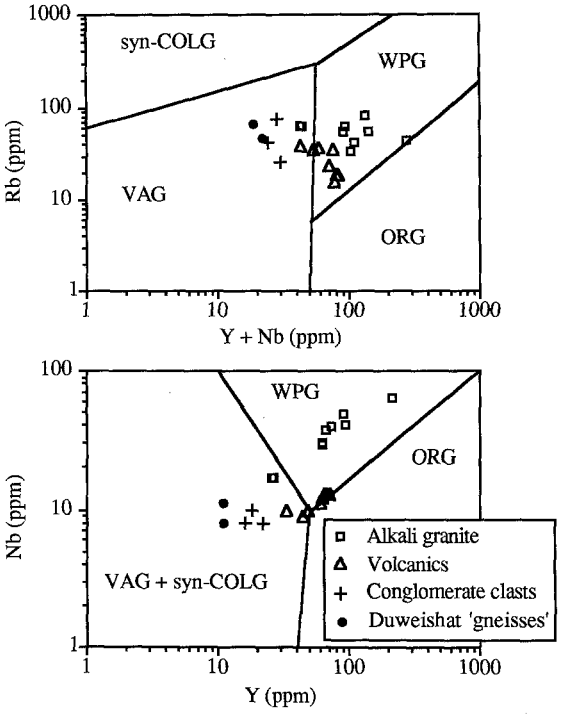

Fig. 4. Trace element discrimination digrams for resolving the tectonic settings of granitic rocks, after Pearce et al. (1984). syn-COLG = Syn-collisional granite; VAG = volcanic arc granite; WPG = within-plate granite; ORG = ocean ridge granite

Neodymium model ages (T_{DM}; Table 5) vary almost as widely as the zircon ages, from 1.3 to 2.8 Ga, and are consistently older than the zircon evaporation ages for the same rocks. Figure 6 compares the ages for the Duweishat gneisses obtained by the three methods. It is apparent from this diagram that much of the scatter in the Rb–Sr data results from the fact that the suite is not of the same age. The zircon ages are consistently younger than the Nd and Sr depleted mantle model ages, as is generally the case in metamorphic terranes, because the latter are, in fact, mean crustal residence ages (Arndt and Goldstein, 1987). The most plausible explanation for the wide range in ages is that rock of different ages were thrust together during intense deformation, and that the preserved gneisses at Duweishat constitute a tectonic sequence in which all primary contacts have been obliterated by high strain.

Nd isotopic data are plotted as a function of age on Fig. 7, showing not only the isotopic composition of Nd at the time of crystallization of the zircons, but also the Nd model age (T_{DM}). The wide range of ages and isotopic compositions is apparent in this figure, and the contrast with the much tighter distribution of ages and isotopic compositions for samples from north-east Sudan. It is also

Fig. 5. Rb–Sr isochron diagrams for samples from the Wadi Halfa study area. (A) Duweishat gneisses. Broken lines labelled 1.4 Ga and 700 Ma are for purposes of reference; (B) volcanic rocks WH 1–6; (C) volcanic rocks WH 29–32; and (D) granites WH 20–28, with WH-23 omitted

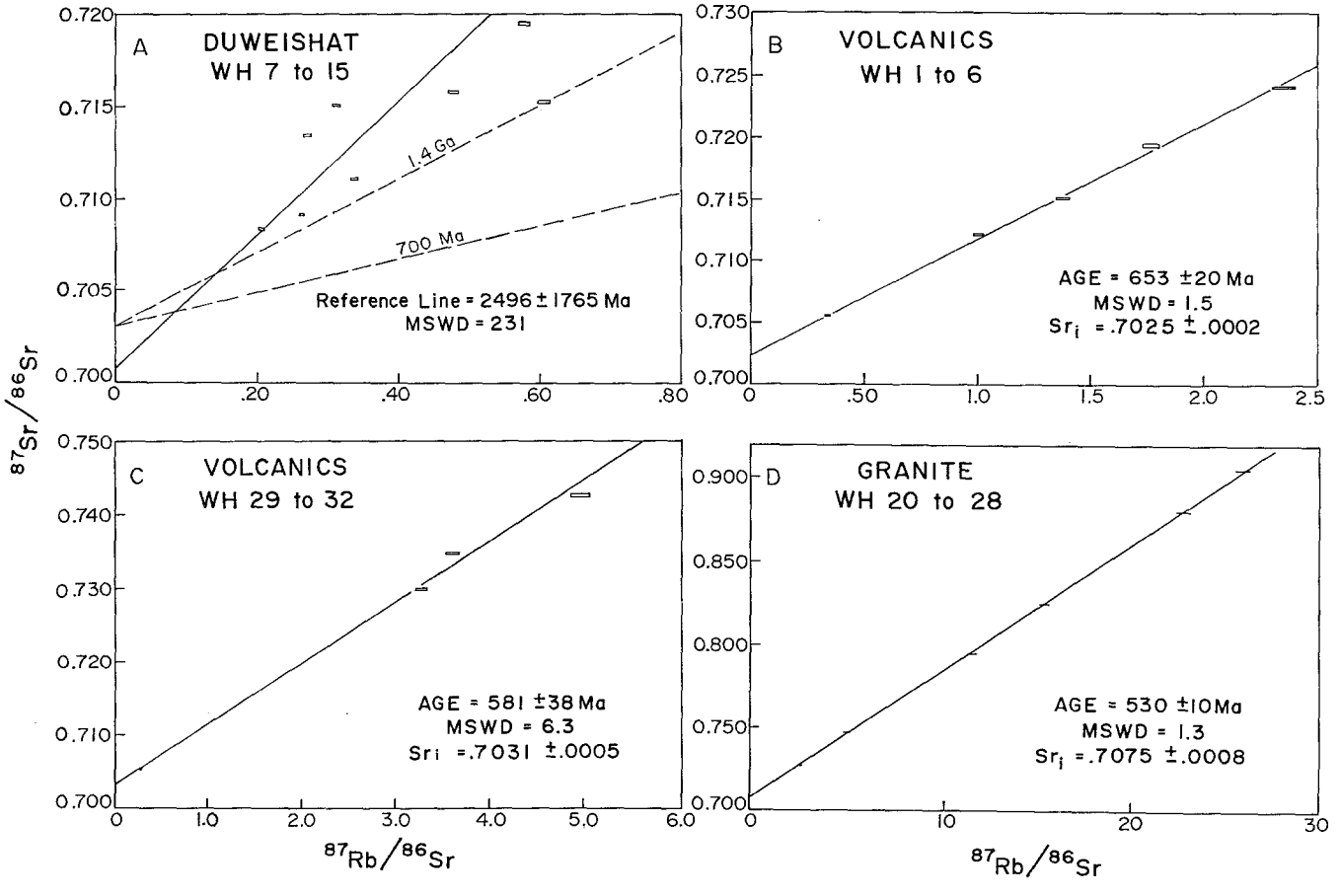

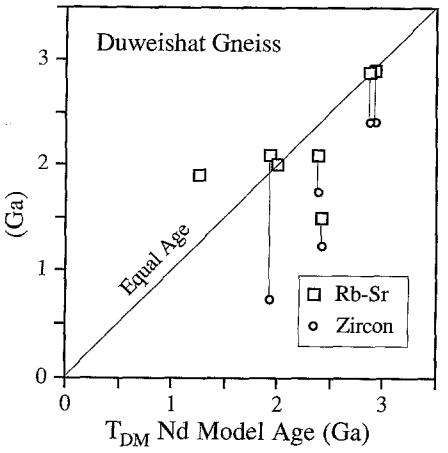

Fig. 6. Comparison of ages for the Duweishat gneisses. Horizontal axis gives T_{DM} Nd model age, whereas the vertical axis gives the zircon evaporation age (circle) or Rb–Sr model age (square; R_i assumed = 0.702). Vertical lines connect Rb–Sr model and zircon ages for the same sample.

apparent from Fig. 7 that the protoliths of the gneisses already had $\varepsilon_{Nd} < 0$ at the time when the zircons formed.

The isotopic composition of Pb in K-feldspars separated from two of the Duweishat gneisses are reported in Table 6. Compared with feldspars analysed from elsewhere in north-east Africa or Arabia, the Duweishat feldspars have extremely unradiogenic $^{206}Pb/^{204}Pb$ coupled with highly radiogenic $^{207}Pb/^{204}Pb$; only one sample from the Afif terrane, Saudi Arabia, has a lower $^{206}Pb/^{204}Pb$ (16.747; Stoeser and Stacey, 1988). This indicates that the lead evolved in an ancient, high U/Pb environment in pre-Neoproterozoic times, but was arrested during the Neoproterozoic. These data also serve to confirm and extend the trend identified for ANS feldspar Pb isotopic compositions (Fig. 8), interpreted to result from mixing between mantle-derived and ancient upper crustal sources (Sultan et al., 1992a).

Fig. 7. Plot of age versus ε_{Nd}. Curve with ticks is model depleted mantle (Nelson and DePaolo, 1985). Closed circles show isotopic composition of each Duweishat gneiss at the age given by zircon evaporation dating; solid lines show evolution of Nd and Nd model age. Note that two samples do not have zircon evaporation ages. Broken lines, square and triangle show similar relationships for the 650 Ma volcanic rocks and 530 Ma alkali granite. Nd model ages (T_{DM}) are the intersection between these straight lines and the model depleted mantle curve. Also shown in stipples is the field defined by the Nd isotopic composition of 17 well dated samples from north–east Sudan (Stern and Kröner, 1993).

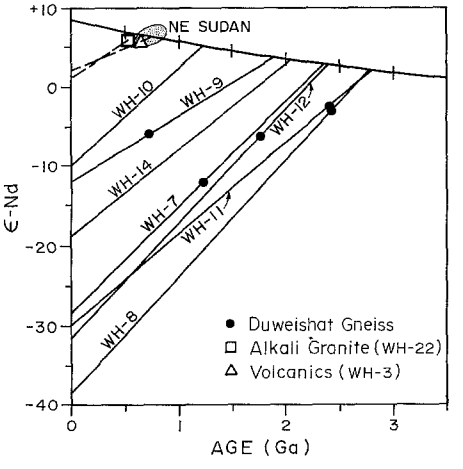

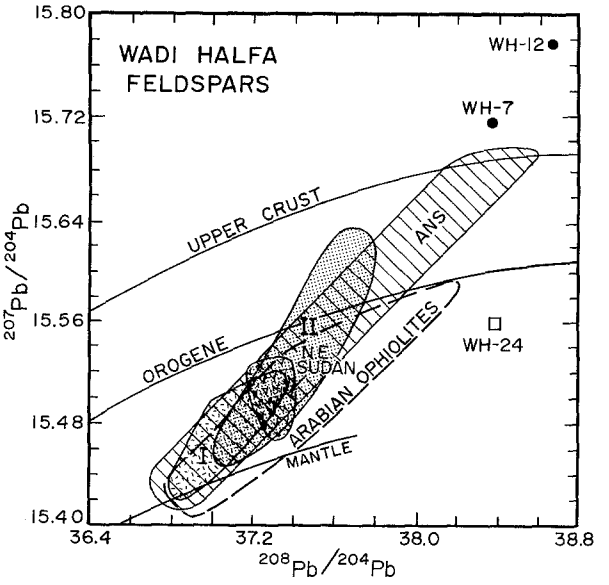

Fig. 8. Plot of $^{207}Pb/^{204}Pb$ versus $^{208}Pb/^{204}Pb$, showing the location of Arabian–Nubian Shield feldspars and galenas (Sultan et al. 1992a). Field occupied by feldspars from Arabian ophiolites is from Pallister et al. (1988). Curves labelled 'mantle', 'orogene' and 'upper crust' are from the plumbotectonics model of Zartmann and Doe (1981). Note that the two samples from the Duweishat gneiss have very radiogenic $^{207}Pb/^{204}Pb$ and $^{208}Pb/^{204}Pb$, but non-radiogenic $^{206}Pb/^{204}Pb$ (Table 6), implying extraction a long time ago from a high Th/U and U/Pb environment, probably ancient upper crust.

Conglomerate

The conglomeratic unit east of the Duweishat gneiss is about 2 m thick and consists of cobbles of gneiss, granite and rhyolite up to 50 cm in greatest dimension. This unit has a strong subhorizontal foliation and cobbles are elongated ENE–WSW. Three cobbles (WH-17–19) of foliated biotite granodiorite were collected. WH-17 and 18 are compositionally similar (Table 2: SiO_2 = 76%, K_2O = 1.7 to 2.3%), whereas WH-19 contains significantly greater concentrations of large ion lithophile elements (K_2O = 3.6%) at lower SiO_2 (69.4%). All three samples plot in the field of 'volcanic arc granites' in Fig. 4. Newertheless, single zircon dating indicate a significant difference in age between WH-17 (718 ± 15 Ma) and WH-19 (2451 ± 5 Ma) (Table 4). Interestingly, both the ca. 720 Ma and ca. 2430 Ma ages are found in the Duweishat gneiss as well as in the conglomerate; this and compositional similarities between the conglomerate and the Duweishat gneisses suggest that the conglomerate may be locally derived. The age of 718 ± 15 Ma provides an older age limit for the unconformity between the gneiss and the supracrustal succession.

Metavolcanic rocks

These rocks were sampled at two localities (Fig. 3). At the first locality (WH-1 – 6) fragmental flows strike 170° with a near-vertical dip. Sample WH-2 is a metabasalt, whereas WH-1 and WH-3 to WH-6 are metarhyolites. At the second locality, very fresh samples WH-29 to WH-31 (rhyolites) were collected with WH-32 (andesite) sampled 3 km to the south – east. These rocks have been metamorphosed to the greenschist facies. The chemical analyses (Table 2) show that the felsic rocks have $SiO_2 > 75\%$ and moderate K (1.2 – 3.4% K_2O).

The tectonic setting of these metavolcanic rocks is enigmatic. On discriminant diagrams designed for granitic rocks (Fig. 4), these plot intermediate between 'volcanic arc granites' and 'within-plate granites'. Bender (1991) noted that on the Nb – Zr discriminant diagram of Leat et al. (1986), these rocks plot in the field for rhyolites of oceanic and continental rift zones. The one basalt sample (WH-2) contains moderately high TiO_2 (1.3%) but low Zr (95 ppm), plotting at the boundary between 'arc' and 'within-plate' mafic magmas in the Ti – Zr discriminant diagram of Pearce (1980).

Both metavolcanic suites were dated using the Rb – Sr whole rock technique. WH-1 – 6 had a good spread in $^{87}Rb/^{86}Sr$ and yielded a six-point isochron (Fig. 5B; MSWD = 1.5) with an age of 653 ± 20 Ma and $R_i = 0.702\,5 \pm 2$. We interpret this to approximate the time of volcanism. WH-29 – 32 also had a good spread in $^{87}Rb/^{86}Sr$ (Fig. 5C), but yielded an errorchron (MSWD = 6.3). We interpret the age of 581 ± 38 Ma for this suite to reflect post-depositional disturbance and will not use this result in any of the subsequent discussion. Note, however, that the low R_i for this suite (0.703 1 ± 5) is similar to that observed for WH-1 – 6.

A felsic sample (WH-3) was analysed for Sm and Nd concentration and Nd isotopic composition (Table 5). This yielded an ε_{Nd} of +6.6 at 650 Ma and T_{DM} = 0.66 Ga, indistinguishable from the age of eruption. Both Sr and Nd isotopic systematics indicate that these volcanics represent juvenile additions to the crust and experienced no discernible contribution from older crust such as the Duweishat gneisses.

Alkali granite

Several bodies of post-tectonic granite intrude the basement around Wadi Halfa. We collected nine samples from four localities in one of the largest of these plutons (Fig. 3). These are orange – pinkish in the field and are predominantly composed of quartz and perthitic K-feldspar. They classify as alkali granite, plot in the field of 'within-plate granites' (Fig. 4), and have compositions that are similar to 'A-type' granites worldwide (Bender, 1991). Seven samples were analysed for Rb – Sr geochronology and six of these used to generate an isochron (MSWD = 1.3) with an excellent spread in $^{87}Sr/^{86}Sr$ (Fig. 5D). Sample WH-23 was omitted because this data point falls grossly off of the isochron. The age of 530 ± 10 Ma is accepted as reflecting the time of intrusion/crystallization of the granite and the moderately high R_i (0.707 5 ± 8) is interpreted as indicating some contamination by older crust. The Nd isotopic results for one sample (WH-22; Table 5) indicate that participation of pre-Pan-African crust in the generation of this granite was limited (ε_{Nd} = +4.9 at 530 Ma and T_{DM} = 0.72 Ga). The isotopic composition of Pb in K-feldspar from one of these samples (WH-24: Table 6; Fig. 8) confirms that participation of older crust in the generation of this alkali granite was minor.

Discussion

In this section we discuss the significance of our results for the understanding of the evolution of this portion of the ESC in this order: (1) the age of the crust of the ESC; (2) timing of tectonic events in north-central Sudan; and (3) insights into the causes of remobilization of the ESC.

Age of the East Saharan craton

One of the problems resulting from the pervasive Neoproterozoic remobilization of the older crust of the ESC is that it is very difficult to know when this crust formed. The Rb – Sr whole rock data indicating an age of 2.6 Ga for the Uweinat massif (Klerkx and Deutsch, 1977) have been confirmed by U/Pb dating of zircons (Sultan et al., 1994). However, the bulk of the pre-Pan-African Nd model ages reported for the ESC in Sudan and Egypt are Proterozoic (Fig. 9), and only a few are Archean. These model ages may either be telling us about the mean age of the crust or result from mixtures between juvenile Neoproterozoic and Archean crust. On the basis of the currently available database it is impossible to determine which interpretation is correct.

Zircons eroded from the ESC may record the age of this older crust. Zircons from clasts in the Atud conglomerate,

Fig. 9. Histogram of T_{DM} Nd model ages for the ESC from Sudan and Egypt. Data sources: Harris et al., 1984; Kröner et al., 1987a; Harms et al., 1990; Sultan et al., 1990. Data from this study are shown as stippled pattern

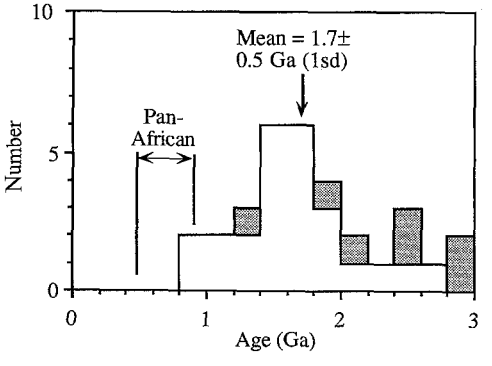

Egypt, yielded upper concordia intercept ages of 1.2–2.3 Ga (Dixon 1979; 1981). Xenocrystic zircons from the Nakhil granite, north-east Egypt, provided upper concordia intercept ages of ca. 1.6 Ga. Ion microprobe dating of single zircons from metasedimentary granulites at Sabaloka, Sudan, yielded three ages: 800–1000 Ma, ca. 2.0 Ga and ca. 2.6 Ga (Kröner et al., 1987a). At Wadi Miyah in Egypt, zircons from Neoproterozoic metasediments yielded evaporation ages of 2410 ± 100 Ma; farther south, detrital zircons from Neoproterozoic metasediments along Wadi Allaqi yielded ages of 1460 ± 100, 2400 ± 140 and 2450 ± 10 Ma, respectively (Wust, 1989). Zircons from igneous rocks of the Western Desert of Egypt have upper concordia intercept ages of 2630, 2060 and 1900–2100 Ma (Sultan et al., 1994). Finally, single zircon ages for the Duweishat gneiss and conglomerate fall into three clusters: ca. 2430, 1740 and 1230 Ma (Table 4). We conclude from this that the history of the ESC began in the late Archean, ca. 2.6 Ga ago, and that this crust experienced significant episodes of crustal growth during the Proterozoic at ca. 2.4, 2.0, 1.6–1.8 and 1.0–1.2 Ga. The range and means of Nd model ages may approximate the age of the pre-Neoproterozoic crust. In some instances, this may reflect fortuitous mixtures of Neoproterozoic mantle-derived magmas with older crust, but the data in hand suggest that the ESC formed at several different times, beginning in the late Archean and continuing throughout the Proterozoic.

Timing of tectonic events in the eastern ESC

A sequence of tectonic events can be inferred from our results and other studies of the basement of northern Sudan and southern Egypt. A cratonic nucleus formed in the late Archean and was subjected to additional crustal growth at several times during the Proterozoic, as outlined above. Sometime before 800 Ma ago, this craton was rifted to form the Mozambique ocean, with the development of an aulacogen-like oceanic re-entrant along the lines of the present Atmur-Delgo ophiolite belt (ADOB in Fig. 3). This re-entrant evolved to form a north–west dipping subduction zone, with an arc on the north–west side of the oceanic basin and a passive margin on the south–east side (Schandelmeier et al., 1994). Subduction continued until at least 731 ± 12, as demonstrated by a $^{207}Pb/^{206}Pb$ zircon age for an I-type granodiorite near Delgo (Harms et al., 1991). A regional north–south shortening event, possibly reflecting collisional orogenesis, is demonstrated by similar times of closure and southward transport of ophiolitic nappes (about 720 Ma) for both the ADOB and the east–west trending Allaqi-Heiani suture along the Sudan–Egypt border to the north–east (Kröner et al., 1992). This deformation and upper greenschist to amphibolite facies metamorphism was probably responsible for the tectonic interleaving of magmatic rocks and their transformation into what is now the Duweishat gneiss. The 719 ± 14 Ma zircon age for WH-9 probably dates the youngest member of this plutonic suite and the above tectonometamorphic event must therefore be younger than this date. We speculate that this tectonic interleaving and thrusting led to crustal thickening and uplift, resulting in erosion and deposition of the conglomerates of Wadi Halfa and the Sulb unit near Delgo (Denkler et al., 1994). This must have occurred early in this deformation episode because these sediments were affected by similar deformation and metamorphism as the gneisses. Amphibolite facies metamorphic rocks of the Sulb unit yielded a Sm–Nd mineral age of ca. 700 Ma (Harms et al., 1994), further constraining peak metamorphism associated with collision.

Eruption of largely subaerial volcanics followed deformation at about 650 Ma. Subduction-induced magmatism on the north side of the Atmur-Delgo-Rahib basin must have stopped at about 700 Ma (dating of amphibolite facies metamorphism and deformation at Delgo). Following regional considerations, we do not interpret the 650 Ma volcanics as forming in an arc. Suturing of terranes within the ANS was largely completed by 700 Ma, as demonstrated by the eruption of voluminous post-collisional Asoteriba intraplate felsic volcanic sequences (Stern and Kröner, 1993). For this reason, we interpret the Halfa volcanics as forming in a post-collisional, intracontinental rift. This interpretation may apply to the Abu Sari unit (Denkler et al., 1994) as well. Regional east–west shortening formed north–south trending, upright folds; this event is probably similar in age and cause to the 610–660 Ma Hamisana D_2 deformation farther E (Stern et al., 1990). Post-tectonic granites were intruded in the region at different intervals after 600 Ma (530 Ma at Halfa, this study; 560–570 Ma at Delgo, Harms et al., 1990; 550 in north-east Bayuda, Ries et al., 1985; 540 Ma at Sabaloka, Kröner et al., 1987a).

Causes of Neoproterozoic remobilization of the ESC

As noted in the introduction, the ESC was pervasively affected by tectonic, metamorphic and igneous events of Neoproterozoic age. A number of suggestions may be made for the origin of this regional disruption of what may or may not have been a craton prior to the Neoproterozoic. As pointed out by Stern (1994), there are three general classes of explanations for such remobilization: (1) convergent margin or collisional processes; (2) extension of the crust and lithosphere; and (3) delamination of subcrustal mantle lithosphere.

In collisional models, west-directed thrusting from the ANS led to crustal thickening (Schandelmeier et al., 1988). One variant of this argues that at least one ocean basin and associated, subduction-related batholiths formed in the interior of North Africa (e.g. Hoggar Mountains of southern Libya; Rogers et al., 1978). We suggest that deformation affecting the Duweishat gneisses and causing their tectonic interleaving, shortening and uplift, resulted from crustal thickening related to collision.

Extensional models have not been generally considered, but crustal extension can subject broad crustal tracts to high heat flow, uplift and intrusion or underplating of melts from the asthenosphere. The classic example of this is the ca. 1000 km wide Basin and Range province of the USA (Eaton, 1982). Large-scale extension brings asthenosphere nearer to the surface (leading to high heat flow, metamorphism and uplift) and the mechanical properties of extended crust allow passage of relatively uncontamin ated magmas to the surface (Lum et al., 1989). Such crustal extension is often associated with A-type granites (Trønner and Brandon, 1992) and a similar relationship is inferred for northern Sudan during the interval 580–540 Ma (Denkler et al., 1994). Large-scale crustal extension is thus an effective way of extensively remobilizing a large region of older crust and it often follows crustal thickening during orogenic collapse (Malavieille and Taboada, 1991). At present, we do not have a good understanding of the strain history of the ESC, but there was clearly extension in north–east Africa about 540–600 Ma ago (Pudlo and Franz, 1993; Stern et al., 1984). There is also an indication for extension associated with voluminous igneous activity at 710 Ma in south-east Egypt (Stern et al., 1991) and the interpretation of the Atmur-Delgo ophiolite belt as an oceanic re-entrant indicates that crustal extension proceeded to the point of seafloor spreading sometime before 750 Ma (Schandelmeier et al. 1994). It is becoming increasingly clear that strong crustal extension has been important in the Neoproterozoic evolution of the region.

The application of models of subcrustal lithospheric delamination to the region is relatively recent. Ashwal and Burke (1989) argued that the continental lithospheric mantle (CLM) beneath North Africa was separated from the crust after thickening as a result of Neoproterozoic collision, thus forming undepleted lithosphere which became the source of intraplate magmas during the Tertiary. Building on this suggestion, Black and Liégeois (1993) proposed that delamination of the ESC mantle lithosphere occurred about 700 Ma ago. Because delamination results in the CLM being replaced by asthenosphere, the isotopic composition of mantle-derived magmas should reflect this (Kay and Kay, 1993) and the transition between crustal melts and asthenospheric melts may date delamination.

The data from the Wadi Halfa region provide some support for the inference that magma sources changed from crustal to asthenospheric sometime around 700 Ma. The 731 ± 12 Ma I-type granodiorite at Delgo clearly reflects the participation of older crustal components [$\varepsilon_{Nd}(t) = -6.3$; $T_{DM} = 1.6$ Ga: Harms et al., 1991]. In contrast, the source of the Halfa volcanics is overwhelmingly asthenospheric [$R_i = 0.7025$; $\varepsilon_{Nd}(t) = +6.6$; $T_{DM} = 0.66$ Ga]. Similarly, although the Halfa alkali granite has an elevated R_i (0.707 5), the Nd isotopic data indicate a predominantly asthenospheric source [$\varepsilon_{Nd}(t) = +4.9$; $T_{DM} = 0.72$ Ga]. Pb isotopic compositions of K-feldspar supports the inference that interaction with the crust was limited. Our limited data are therefore compatible with the conclusion that magma sources changed from predominantly crustal to predominantly asthenospheric sometime between 730 and 650 Ma. This is also consistent with the suggestion of Kröner et al. (1987a) that granulite facies metamorphism at Sabaloka at 720 Ma was accompanied by the emplacement of mafic magmas in the lower crust. With the meagre database existing for the ESC, we cannot determine whether similar source transitions are found throughout the region and if so, whether this reflects lithospheric delamination or a change from a collisional to an extensional tectonic environment.

It should be clear from the foregoing discussion that there was probably no single cause for the Neoproterozoic remobilization of the ESC. There is evidence for crustal extension as well as for collision. It is difficult to evaluate the role that delamination might have had because these effects are difficult to distinguish from the effects of rifting and collision. If were are to decipher the protracted and complex history of the ESC during its Neoproterozoic evolution, we must obtain better temporal constrains on evolving magma sources and deformational styles and timing.

Conclusions

Exposures around Wadi Halfa lead to new insights the Neoproterozoic evolution of the foreland to the Arabian–Nubian Shield and its relationship to processes of juvenile crust formation in this shield. The most important of these conclusions are:

1. Several episodes of crustal formation and/or reworking of older crust can be identified within the Duweishat gneisses. Single zircon evaporation analyses yield ages of 0.72, 1.23, 1.74 and 2.4 Ga, whereas Nd isotopic data yield T_{DM} ages of 1.3, 1.9–2.0, 2.4 and 2.8 Ga. These data indicate that the ESC in Egypt and Sudan mostly formed during the interval 2.8–1.2 Ga, but with the addition of abundant but unknown proportions of juvenile material during Neoproterozoic time.
2. Complex deformation, including mylonitization, to assemble the varied components of the Duweishat gneisses occurred about 720 Ma ago, probably reflecting a plate collision event. This deformation was succeeded by an interval of erosion that occurred between 720 and 650 Ma ago.
3. Intraplate rifting and volcanism at ≈ 650 Ma involved melting of asthenospheric mantle.
4. An episode of east–west shortening, similar to that in the Hamisana shear zone to the east, occurred between 650 and 540 Ma ago. Regional considerations further constrain this event to between 650 and 610 Ma.
5. Our results are compatible with the hypothesis of regional delamination of the subcontinental mantle

beneath the ESC at about 700 Ma, but these effects cannot be distinguished from tectonic and magmatic changes expected from the transition between collision and rifting.

6. Remobilization of the ESC during the Neoproterozoic was a long and complex process that included a significant proportion of juvenile crustal growth. Juvenile crustal growth is made most obvious through the preservation of ophiolites and in post-700 Ma igneous rocks.

Acknowledgements We appreciate funding by the German Research Council (DFG), grant Kr 590/11, the Volkswagen Foundation and the German Ministry of Economic Cooperation (BMZ) as well as grants from NASA to RJS. AK acknowledges analytical facilities in the Max-Planck-Institut für Chemie in Mainz. The comments of H. Schandelmeier and M. Sultan are gratefully acknowledged. A. A. Rashwan made available maps of the then Geological and Mining Centre, Area of Integration, Aswan, Egypt. Finally, we thank the police and unnamed friends in Wadi Halfa who helped to obtain petrol for our field vehicles during an economically difficult period in the Sudan. This is UTD Programs in Geosciences contribution # 776.

References

Arndt NT, Goldstein SL (1987) Use and abuse of crust-formation ages. Geology 15: 893–895

Ashwal LD, Burke K (1989) African lithospheric structure, volcanism and topography. Earth Planet Sci Lett 96: 8–14

Bender R (1991) Petrographische und geochemische Untersuchungen präkambrischer Gesteine des zentralen Nordsudan. Unpubl Diploma Thesis. Univ. Mainz, 133 pp

Bertrand JM, Caby R (1978) Geodynamic evolution of the Pan-African orogenic belt: a new interpretation of the Hoggar shield (Algerian Sahara). Geol Rundsch 67: 357–388

Black R, Liégeois J-P (1993) Cratons, mobile belts, alkaline rocks and continental lithospheric mantle: the Pan-African testimony. J Geol Soc London 150: 89–98

Camp VE (1984) Island arcs and their role in the evolution of the western Arabian Shield. Geol Soc Am Bull 95: 913–921

Denkler T, Franz G, Schandelmeier H (1994) Tectono-metamorphic evolution of the Neoproterozoic Delgo suture zone, Northern Sudan. Geol Rundsch 83: 578–590

Dixon TH (1979) The evolution of continental crust in the Late Precambrian Egyptian Shield. Unpubl PhD Thesis. Univ California San Diego, 229 pp

Dixon TH (1981) Age and chemical characteristics of some pre-Pan-African rocks in the Egyptian Shield. Precambrian Res 14: 119–133

Eaton GP (1982) The Basin and Range Province: origin and tectonic significance. Annu Rev Earth Planet Sci 10: 409–440

Griffiths PS, Curtis PAS, Fadul SEA, Scholes PD (1987) Reconnaissance geological mapping and mineral exploration in northern Sudan using satellite remote sensing. Geol J 22: 225–249

Harms U, Schandelmeier H, Darbyshire DPF (1990) Pan-African reworked early/middle Proterozoic crust in NE Africa west of the Nile: Sr and Nd isotope evidence. J Geol Soc London 147: 859–872

Harms U, Hengst F, Pilot J (1991) ($^{207}Pb/^{206}Pb$)* single zircon age determinations and Sr and Nd isotope investigations on Upper Proterozoic granitoids from N-Sudan (abstract). Isotope Coll Freiberg 4: 16

Harms U, Darbyshire DPF, Denkler T, Hengst M, Schandelmeier H (1994) Evolution of the Neoproterozoic Delgo suture zone and crustal growth in northern Sudan: Geochemical and radiogenic isotope constraints. Geol Rundsch 83: 591–603

Harris NBW, Hawkesworth CJ, Ries, AC. (1984) Crustal evolution in north-east and East Africa from model Nd ages. Nature 309: 773–776

Kay RW, Kay SM (1993) Delamination and delamination magmatism. Tectonophysics 219: 177–189

Klerkx J, Deutsch S (1977) Resultats preliminaires obtenus par la method Rb/Sr sur l'age des formations Precambriennes de la region d'Uweinat (libye). Mus R Afr Centr Tervuren (Belg) Dépt Géol Min Rapp Ann 1976: 83–94

Kober B (1986) Whole-grain evaporation for $^{207}Pb/^{206}Pb$ investigation on single zircons using a double-filament thermal ion source. Contrib Mineral Petrol 93: 482–490

Kober B (1987) Single-zircon evaporation Pb^+ emitter-bedding for $^{207}Pb/^{206}Pb$ investigations using thermal ion mass spectrometry, and implications to zirconology. Contrib Mineral Petrol 96: 63–71

Krogh TE (1973) A low-contamination method for hydrothermal decomposition of zircon and extraction of U and Pb for isotopic age determinations. Geochim Cosmochim Acta 37: 485–494

Kröner A (1977) The Precambrian geotectonic evolution of Africa: plate accretion vs. plate destruction. Precambrian Res. 4: 163–213

Kröner A, Stern RJ, Dawoud AS, Compston W, Reischmann T (1987a) The Pan-African continental margin in northeastern Africa: Evidence from a geochronological study of granulites at Sabaloka, Sudan. Earth Planet Sci Lett 85: 91–104

Kröner A, Greiling R, Reischmann T, Hussein IM, Stern RJ, Dürr S, Krüger J, Zimmer M (1987b) Pan-African crustal evolution in the Nubian segment of Northeast Africa. In: Kröner A (ed) Proterozoic Lithospheric Evolution. Am Geophys Union Geodyn Ser 17: 235–257

Kröner A, Todt W, Hussein IM, Mansour M (1992) Dating of late Proterozoic ophiolites in Egypt and the Sudan using the single grain zircon evaporation technique. Precambrian Res 59: 15–32

Leat PT, Jackson SE, Thorpe RS, Stillman CJ (1986) Geochemistry of bimodal basalt-subalkaline/peralkaline rhyolite provinces within the Southern British Caledonides. J Geol Soc London 143: 259–273

Lum CCL, Leeman WP, Foland KA, Kargell JA, Fitton JG (1989) Isotopic variations in continental basaltic lavas as indicators of mantle heterogeneity: examples from the western U.S. Cordillera. J Geophys Res 94: 871–884

Malavieille J, Taboada A (1991) Kinematic model for postorogenic Basin and Range extension. Geology 19: 555–558

Nelson BK, DePaolo DJ (1985) Rapid production of continental crust 1.7 to 1.9 b.y. ago: Nd isotopic evidence from the basement of the North American midcontinent. Geol Soc Am Bull 96: 746–754

Pallister JS, Stacey JS, Fischer LB, Premo WR (1988) Precambrian ophiolites of Arabia: geologic setting, U–Pb geochronology, Pb-isotope characteristics, and implications for continental accretion. Precambrian Res 38: 1–54

Pankhurst RJ, O'Nions RK (1973) Determination of Rb/Sr and $^{87}Sr/^{86}Sr$ ratios of some standard rocks and evaluation of X-Ray fluorescence spectrometry in Rb–Sr geochemistry. Chem Geol 12: 127–136

Pearce JA (1980) Geochemical evidence for the genesis and eruptive setting of lavas from Tethyan ophiolites. Proc Ophiolite Symp Nicosia, Cyprus: 261–272

Pearce JA, Harris NBW, Tindle AG (1984) Trace element discrimination diagrams for the tectonic interpretation of granitic rocks. J Petrol 25: 956–983

Pier JG, Podosek PA, Luhr JF, Brannon JC, Aranda-Gomez JJ (1989) Spinel-lherozolite-bearing Quaternary volcanic centers in San Luis Potosi, Mexico. 2. Sr and Nd isotopic systematics, J Geophys Res 94: 7941–7951

Pudlo D, Franz G (1993) Late Panafrican dyke rocks in the Bir Safsaf complex, Western Desert Egypt [abstract]. In: Thorweihe

U, Schandelmeier H (eds) Geoscientific Research in Northeast Africa, Ballkema, Rotterdam, pp 67–71

Richard P, Shimizu N, Allegre CJ (1976) $^{143}Nd/^{146}Nd$, a natural tracer. An application to oceanic basalts. Earth Planet Sci Lett 31: 269–278

Ries AC, Shackleton RM, Dawoud AS (1985) Geochronology, geochemistry and tectonics of the NE Bayuda Desert, N Sudan: implications for the western margin of the late Proterozoic fold belt of NE Africa. Precambrian Res 30: 43–62

Rocci, G (1965) Essai d'interprétation de mésures géochronologiques. La structure de l'Ouest africain. Sci Terre Fr 10: 461–479

Rogers JW, Ghuma MA, Nagy RM, Greenberg JK, Fullagar PD (1978) Plutonism in Pan-African belts and the geologic evolution of northeastern Africa. Earth Planet Sci Lett 39: 109–117

Schandelmeier H, Richter A, Harms U (1987) Proterozoic deformation of the East Saharan craton in southeast Libya, south Egypt, and north Sudan. Tectonophysics 140: 233–246

Schandelmeier H, Darbyshire DPF, Harms U, Richter A (1988) The East Saharan Craton: evidence for pre-Pan-African crust in NE Africa west of the Nile. In: El Gaby S, Greiling R (eds) The Pan African Belt of NE Africa and Adjacent Areas. Earth Evol Sci. Vieweg, Wiesbaden, pp 69–94

Schandelmeier H, Wipfler E, Küster D, Sultan M, Stern RJ, Abdelsalam MG. Atmur-Delgo suture: A Neoproterozoic oceanic basin extending into the interior of northeast Africa. Geology 22: 563–566

Stacey JS, Hedge CE (1984) Geochronologic and isotopic evidence for early Proterozoic crust in the eastern Arabian Shield. Geology 12: 310–313

Stern RJ. (1994) Arc assembly and continental collision in the Neoproterozoic East African orogen: Implications for the consolidation of Gondwanaland. Annu Rev Earth Planet Sci 22: 319–351

Stern RJ, Hedge CE (1985) Geochronologic and isotopic constraints on late Precambrian crustal evolution in the Eastern Desert of Egypt. Am J Sci 285: 97–127

Stern RJ, Kröner A (1993) Late Precambrian crustal evolution in NE Sudan: isotopic and geochronologic constraints. J Geol 101: 555–574

Stern RJ, Gottfried D, Hedge CE (1984) Late Precambrian rifting and crustal evolution in the northeastern Desert of Egypt. Geology 12: 168–172

Stern RJ, Nielsen KC, Best E, Sultan M, Arvidson RE, Kröner A (1990) Orientation of late Precambrian sutures in the Arabian–Nubian shield. Geology 18: 1103–1106

Stern RJ, Kröner AK, Rashwan AA (1991) A late Precambrian (~ 710 Ma) high volcanicity rift in the southern Eastern Desert of Egypt. Geol Rundsch 80: 155–170

Stern RJ, Abdelsalam MG, Schandelmeier H, Sultan M, Wickham S (1993) Carbonates of the Keraf zone, NE Sudan: a neoproterozoic (ca. 750 Ma) passive margin on the eastern flank of West Gondwanaland? Geol Soc Am Abstr Progr 25: 49

Stoeser DB, Stacey JS (1988) Evolution, U–Pb geochronology, and isotope geology of the Pan-African Nabitah orogenic belt of the Saudi Arabian Shield. In: El-Gaby S, Greiling RO (eds) The Pan-African Belt of northeast Africa and Adjacent Areas. Earth Evol. Sci. Vieweg Sohn, Wiesbaden, pp 227–288

Sultan M, Tucker RD, El Alfy Z, Attia R, Ragab AG (1994) U–Pb (zircon) ages for the gneissic terrane west of the Nile, Southern Egypt. Geol Rundsch 83: 514–522

Sultan M, Chamberlain KR, Bowring SA, Arvidson RE, Abuzeid H, El Kaliouby B (1990) Geochronologic and isotopic evidence for involvement of pre-Pan-African crust in the Nubian shield, Egypt. Geology 18: 761–764

Sultan M, Bickford ME, El Kaliouby B, Arvidson RE (1992a) Common Pb systematics of Precambrian granitic rocks of the Nubian shield (Egypt) and tectonic implications. Geol Soc Am Bull 104: 456–470

Sultan M, Tucker RD, Gharbawi RI, Ragab AI, El Alfy Z (1992b) On the extension of the Congo craton into the Western Desert of Egypt. Geol Soc Am Abstr Progr 24: A138

Trønner RG, Brandon AD (1992) Mildly peraluminous high-silica granites in a continental rift: the Drammen and Finnemarka batholiths, Oslo Rift, Norway. Contrib Mineral Petrol 109: 275–294

Vail JR (1976) Outline of the geochronology and tectonic units of the basement complex of northeast Africa. Pro R Soc London A 350: 127–141

Vail JR, Dawoud AS, Ahmed F (1973) Geology of the third cataract, Halfa District, Northern Province, Sudan. Geol Min Res Dept Sudan Bull 22: 34 pp

Wust H-J (1989) Geochronologie und Geochemie präkambrischer Metasedimente und Metavulkanite der südlichen Eastern Desert, Ägypten. Unpubl Diploma Thesis. Univ Mainz: 79 p

Wust H-J, Todt W, Kröner A (1987) Conventional and single grain zircon ages for metasediments and granite clasts from the Eastern Desert of Egypt: evidence for active continental margin evolution in Pan-African times [abstract]. Terra Cognita 7: 333–334

York D (1969) Least squares fitting of a straight line with correlated errors. Earth Planet Sci Lett 5: 320–324

Zartman RE, Doe BR (1981) Plumbotectonics – the model. Tectonophysics 75: 136–162